Proceedings of the International Gas Turbine Congress 2003 Tokyo
November 2-7, 2003

IGTC2003Tokyo OS-104

Numerical Analysis of 2.5 Dimensional Geometry Turbine Performance

Naoki WATANABE, Susumu TERAMOTO and Toshio NAGASHIMA

Department of Aeronautics and Astronautics
University of Tokyo
7-3-1 Hongo, Bunkyo-ku, Tokyo 113-8656, JAPAN
Phone: +81-3-5841-6623, FAX: +81-3-5841-6623, E-mail: naoki@thermo.t.u-tokyo.ac.jp

ABSTRACT

There are many difficulties in realizing Ultra-micro gas-turbine system. Among them, the effects of Reynolds number and heat transfer upon the turbine flowfield are discussed in this paper. The flowfield inside the turbine stage composed of blades without twist was investigated numerically with the Reynolds-averaged three-dimensional thin-layer Navier-Stokes equations. Decrease of Reynolds number makes boundary layer thicker and deteriorates the stage efficiency. However, no other remarkable changes were found on flowfield with decreased Reynolds number. Heat transfer, on the other hand, has two kinds of effect on the turbine stage. First, it gives a change in the velocity at the nozzle outlet and deviates the relative flow angle at the rotor inlet, which influences the stage characteristics considerably. Second, heat transfer at the wall has impact on the development of the boundary layer on the blade surface. It was found that the boundary layer more easily separates over the cooled wall than the adiabatic wall.

INTRODUCTION

An unique "shirt button sized gas turbine" concept was presented by MIT researchers (Epstein, et al., 1997). It was a project to minimize gas turbine down to several centimeters, aiming compact electric power source which has power density far higher than conventional batteries. They planned to manufacture gas turbines based on MEMS (Micro Electro Mechanical Systems) technology. Due to manufacturing restriction, blades have constant profile in spanwise direction and only blade height is variable. We call this structure "2.5 dimensional geometry" hereafter.

After Epstein, there have been many efforts in this field. However, there are still many difficulties to be overcome before realizing such micro gas turbines, for example, manufacturing process, material, bearing support and combustion. There are also several aerodynamic concerns.

- Tip Clearance
  It is very difficult to control the tip clearance in miniaturized gas turbines and, as the scale of aerodynamic components becomes smaller, the tip clearance becomes relatively larger.
- Decrease of Reynolds number
  Relatively thicker boundary layer and laminarization due to the decrease of Reynolds number may have a large impact on the flowfield inside gas turbines.
- Heat Transfer
  The temperature of each part of the gas turbine becomes almost uniform due to very small Biot number and the influence of heat transfer upon the flowfield is not negligible with steep temperature gradient.

The objective of the current study is to discuss,

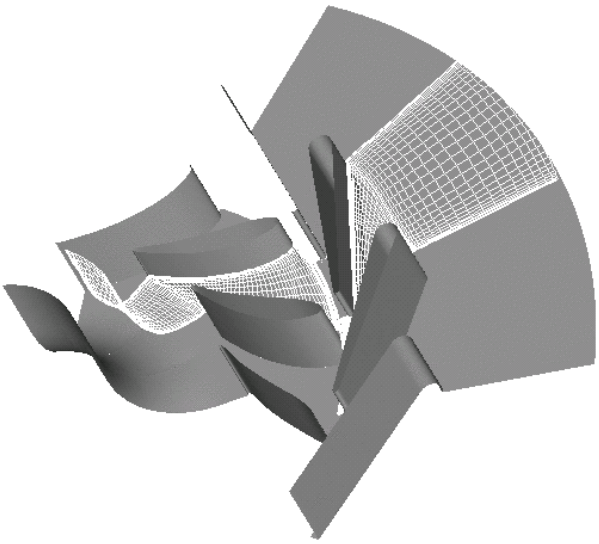

Fig.1: Grid outline

Copyright ©2003 by GTSJ
Manuscript Received on April 30, 2003

Table 1: Design characteristics

rotational speed	240,000 rpm
pressure ratio	2.5
mass-flow rate	30 g/sec
speed ratio	$U/C_0 \simeq 0.63$
inlet total temperature	1223K
specific heat ratio	1.35
gas constant	287.4 J/kg/K
Nozzle	
outer diameter	52 mm
inner diameter	42 mm
number of blades	17
blade height	4.8 mm
Reynolds number	3.21×10^4
Rotor	
outer diameter	40 mm
inner diameter	26 mm
number of blades	15
blade height	4.8 mm
Reynolds number	2.42×10^4

amongst the above, the effects of Reynolds number and heat transfer upon the flowfield inside 2.5 dimensional turbine, hence to improve basic understandings about the flowfield relating to the micro gas turbines.

TARGET AND APPROACH

The turbine studied in this report is a 2.5 dimensional geometry turbine designed and tested by Kato (Kato, et al., 2002). Table 1 shows the design characteristics (Reynolds number is based on inlet density, peripheral velocity, and millimeter). It is approximately ten times larger than Epstein's "shirt button sized gas turbine", referred to "ϕ40 model" hereafter. "ϕ4 model" was also studied, which has the same geometry but one tenth scale of the "ϕ40 model". Reynolds number effect will be discussed by comparing the flowfields between ϕ40 model and ϕ4 model.

Adiabatic wall assumption is usually applied for the numerical analysis of large scale gas turbines, in which heat transfer at the wall has little influence on the structure of the flowfield due to the low heat conduction rate between components. However, for small-scale system like "shirt button gas turbine", heat conduction rate between components is much larger and the temperature of material becomes almost uniform. Therefore, heat transfer effect can be discussed by applying the condition of isothermal wall, which is more realistic for the small-scale analysis.

The calculation cases studied in this report are therefore divided as follows.

- ϕ40 model adiabatic wall
- ϕ40 model isothermal wall
- ϕ4 model adiabatic wall
- ϕ4 model isothermal wall

Several wall temperatures between $700K$ and $900K$ were tested in preliminary study. That range is determined assuming realistic metal temperature. Among them, only the results at $700K$, which show the largest temperature effect, will be discussed in this report. U/C_0 (the ratio of peripheral velocity U to theoretical isentropic expansion velocity C_0) is used as a parameter of operation condition, which is varied within the range from 0.4 to 0.8.

The stage performance will be discussed with adiabatic efficiency η_{ad} and polytropic efficiency η_{pol}. Adiabatic efficiency η_{ad} is defined as follows,

$$\eta_{ad} = \frac{W}{\dot{m} C_p T_{01} \left\{ 1 - \left(\frac{p_3}{P_{01}} \right)^{\frac{\gamma-1}{\gamma}} \right\}} \tag{1}$$

where suffix 0, 1, and 3 represents stagnation condition, nozzle inlet, and rotor outlet respectively. W represents the turbine work output, which is calculated by integrating pressure and shear stress over the rotor blade.

Assuming that polytropic efficiency is constant throughout the rotor passage, the following relation is derived under adiabatic wall condition,

$$\frac{T_{03}}{T_{02}} = \left(\frac{P_{03}}{P_{02}} \right)^{\frac{\eta_p(\gamma-1)}{\gamma}} \tag{2}$$

where suffix 2 represents the rotor inlet. Equation (2) does not take into account heat transfer, while it is extended to include heat transfer effect(Ribaud, 2003). Here, λ is defined as the ratio between heat transfer Q and turbine work output W. Assuming that λ is constant from inlet to outlet, the following equations are derived.

$$\lambda \equiv \frac{Q}{W} \simeq \frac{dQ}{dW} \tag{3}$$

$$\frac{T_{03}}{T_{02}} = \left(\frac{P_{03}}{P_{02}} \right)^{\frac{\eta_p(\gamma-1)(1+\lambda)}{\gamma}} \tag{4}$$

Note that η_p is defined using stagnation properties of both inlet and outlet. Therefore, η_p is regarded as a measure of soundness of the flowfield. However, this definition of polytropic efficiency is based on the assumption that $\frac{dQ}{dW}$ is constant throughout the flowfield. As discussed later, the polytropic efficiency defined from Eq.(4) tends to give higher efficiency for cooled wall.

NUMERICAL METHOD

The governing equations employed here are the Reynolds-averaged three-dimensional thin-layer Navier-Stokes equations. Numerical fluxes for the convective terms are evaluated by the simple high-resolution upwind scheme (SHUS)(Shima, et al., 1997), which is extended to higher order by the MUSCL interpolation based on the primitive variables. The lower-upper alternating directional implicit (LU-ADI) factorized implicit algorithm(Obayashi, et al., 1986) is employed for time integration.

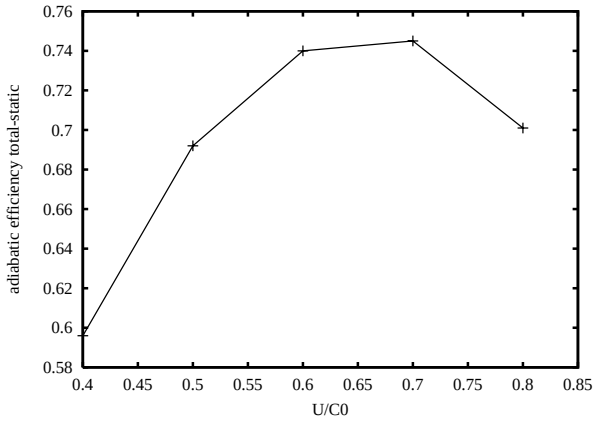

Fig.2: Adiabatic efficiency of $\phi 40$ model with adiabatic wall

Reynolds number is 10^4 to 10^5 for $\phi 40$ model. The flowfield is thus considered to be fully turbulent, and Baldwin-Lomax's algebraic turbulence model(Baldwin and Lomax, 1978) is applied near the solid wall for $\phi 40$ model. For $\phi 4$ model, on the other hand, Reynolds number is 10^3 to 10^4. The flowfield is considered to be laminar and no turbulence model is applied.

Outline of the computational grid used in the simulation is illustrated in Figure 1. Though the figure illustrates three pitches, the simulation area is one pitch of blade-blade flow path. The grid is ($88 \times 35 \times 35$:$\phi 4$, $88 \times 51 \times 51$:$\phi 40$) in the nozzle region and ($83 \times 35 \times 35$:$\phi 4$, $88 \times 51 \times 51$:$\phi 40$) in the rotor region with H-H topology. The minimum grid spacing near the wall is $1.0 \times 10^{-7} m$ for $\phi 4$ model and $2.0 \times 10^{-7} m$ for $\phi 40$ model, so that y^+ is less than unity. Tip clearance between rotor and casing is not considered.

At the nozzle inlet boundary, total pressure and total temperature are fixed, and flow angle is given as radial inflow. At the exducer outlet boundary, static pressure distribution is given by assuming simple radial equilibrium. The blade surface and hub surface of the rotor are rotating around the axis and non-slip wall condition is applied over all solid walls. Thermal condition of the wall is, as stated previously, either adiabatic or isothermal. Periodic condition is applied for the pitchwise boundaries other than the blade surfaces. At the zonal interface between the nozzle and rotor, grid lines are overlapped by three points and the mixing plane method is applied, in which physical quantities are averaged in the pitch direction and exchanged between the zones. Steady analysis is carried out with this method.

RESULTS

Overview

Before going into the discussion about the effect of Reynolds number and wall temperature, overview of the flowfield inside 2.5 dimensional turbine will be explained. $\phi 40$ model with adiabatic wall is taken as a representative case.

Figure 2 shows adiabatic efficiency. The peak efficiency is achieved between 0.6 and 0.7, and the efficiency drops at the higher and lower velocity ratio.

The details of the flowfield and the sources of loss will be discussed in the following sections.

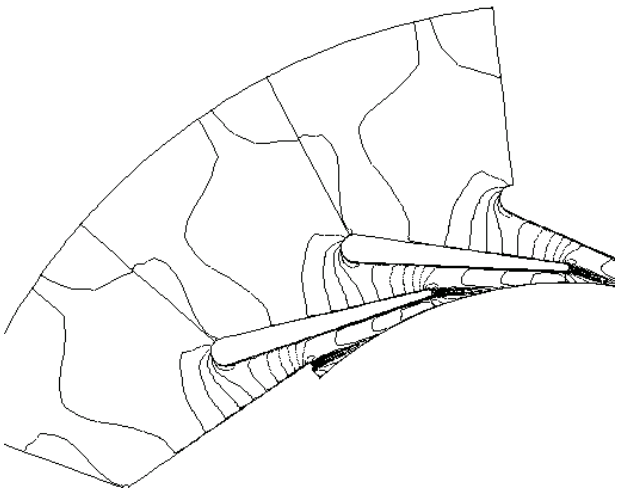

Fig.3: Mach number contours at the nozzle midspan ($U/C_0 = 0.6$)

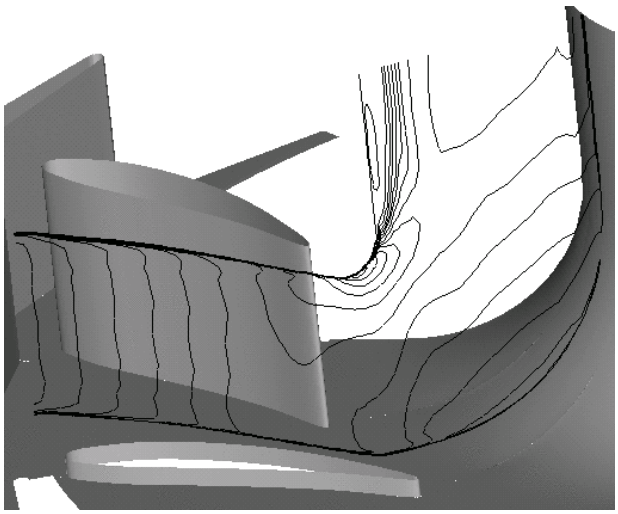

Fig.4: Mach number contours at the exducer midpitch ($U/C_0 = 0.6$)

Nozzle loss Figure 3 shows absolute Mach number at the nozzle midspan. The flow accelerates continuously, and any separation of the boundary layer is not observed. Main source of loss at the nozzle is the wake formed downstream of the thick trailing edge.

Exducer loss Exducer loss is an inherent problem of 2.5 dimensional turbine. Figure 4 shows absolute Mach number at the exducer midpitch. The flow is directed radially inward at the rotor outlet and it is turned to axial direction at the exducer. The curvature radius near the casing is so small that the flow cannot turn completely and separates at this region. Large part of loss at the exducer is caused by this separation.

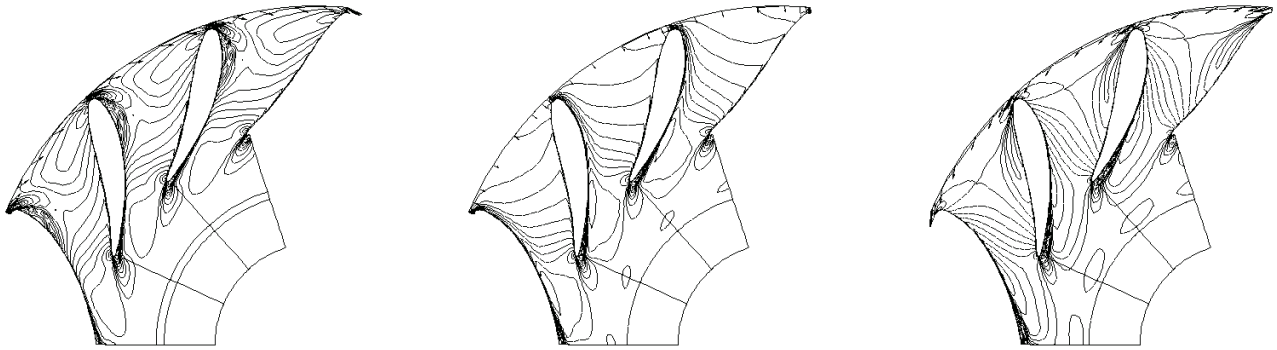

(a): $U/C_0 = 0.4$ (b): $U/C_0 = 0.6$ (c): $U/C_0 = 0.8$

Fig.5: Relative Mach number contours at the rotor midspan

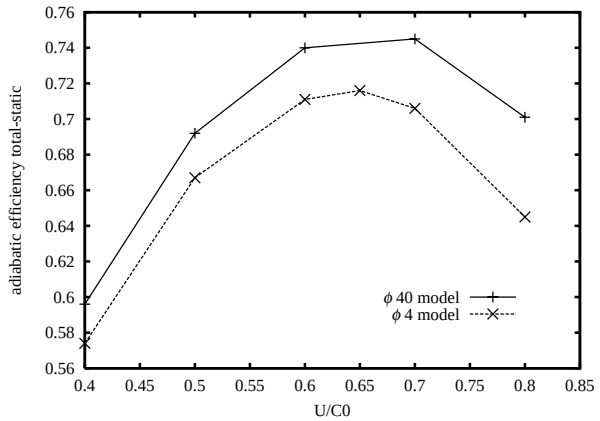

Fig.6: Adiabatic efficiency of $\phi 40$ and $\phi 4$ models (Reynolds number effect)

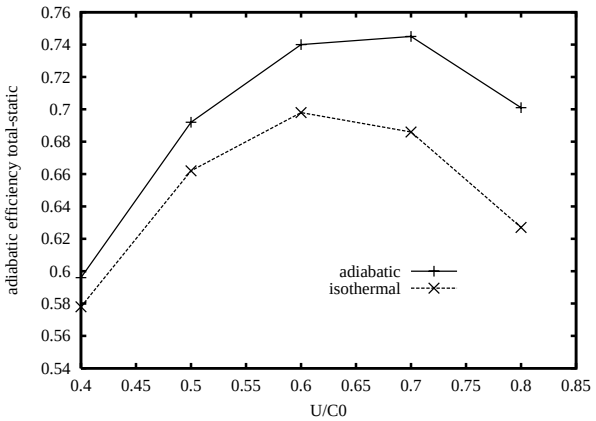

Fig.8: Adiabatic efficiency of $\phi 40$ model (Wall temperature effect)

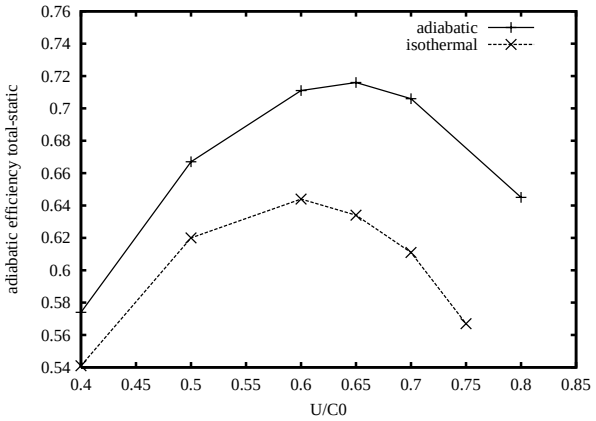

Fig.9: Adiabatic efficiency of $\phi 4$ model (Wall temperature effect)

Rotor loss Figure 5 shows relative Mach number contours at the rotor midspan for three different U/C_0. Relative velocity vectors at the inlet boundary are also illustrated in the figures. The vectors indicate that the inlet flow angle is positive at the lower velocity ratio (Fig.5(a)), while it is negative at the higher velocity ratio (Fig.5(c)). Separation region is observed near the leading edge of the suction surface at low velocity ratio, and on the pressure surface at high velocity ratio. Another separation region also exists near the trailing edge of the suction surface at all velocity ratios.

The extent of the separation regions are consistent with the efficiency curve shown in Figure 2. The efficiency depends mainly on the rotor loss caused by the flow separation.

Effect of Reynolds Number

The effect of Reynolds number upon the flowfield is discussed by comparing $\phi 4$ model and $\phi 40$ model with adiabatic wall. As mentioned before, Reynolds number is 10^4 to 10^5 for $\phi 40$ model and 10^3 to 10^4 for $\phi 4$ model. Figure 6 compares adiabatic efficiency between two models. The efficiency of $\phi 4$ model is lower than that of $\phi 40$ model at all conditions.

Figure 7 shows Mach number contours at the midspan (absolute Mach number and relative Mach number are plotted for the nozzle and the rotor, respectively). The boundary layer and the wake is relatively thicker at $\phi 4$ model than $\phi 40$ model as the result of lower Reynolds number. However, no remarkable difference other than the boundary layer thickness is observed in the flowfield. Primary cause of the difference in efficiency between two cases is therefore due to the boundary layer thickness.

Effect of Wall Temperature

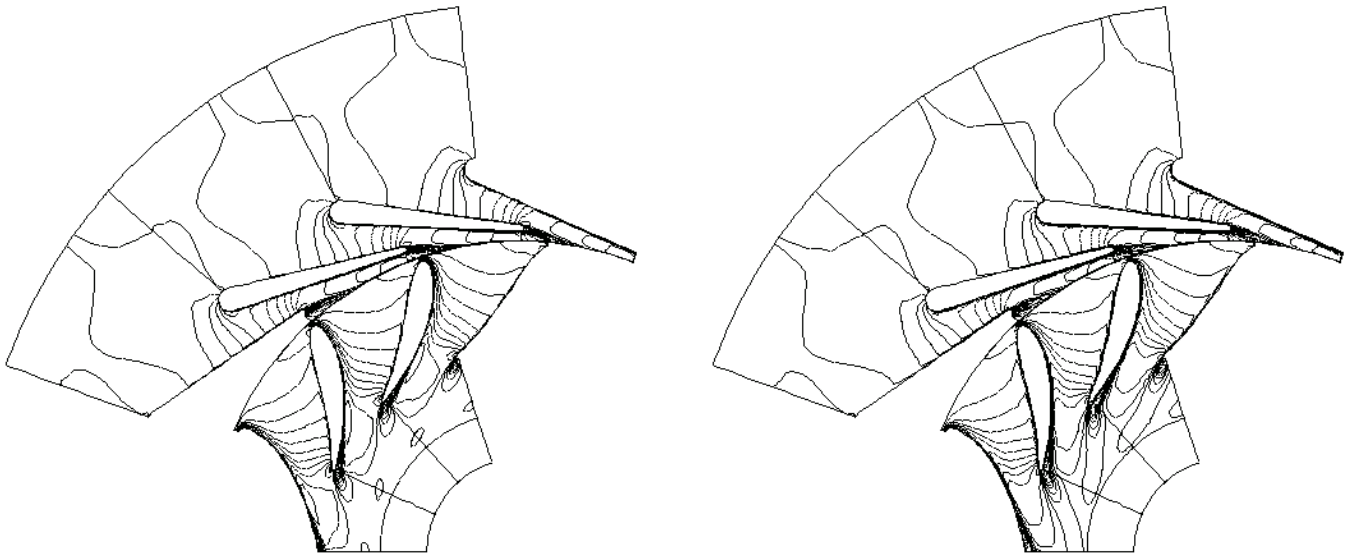

(a): $\phi 40$ model (b): $\phi 4$ model

Fig.7: Mach number contours at the midspan section (Reynolds number effect)

Table 2: Work output and heat transfer ($U/C_0 = 0.6$)

	$\phi = 40$ adiabatic	$\phi = 40$ isothermal	$\phi = 4$ adiabatic	$\phi = 4$ isothermal
Work(W)	6625	6407	61.87	58.60
Heat transfer in Nozzle (W)	0	1847	0	36.53
Heat transfer in Rotor (W)	0	707	0	12.50
Total Heat transfer (W)	0	2554	0	49.03

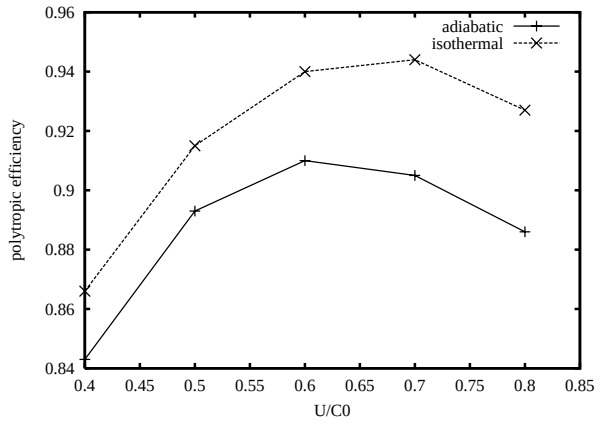

Fig.10: Polytropic efficiency of $\phi 40$ model (Wall temperature effect)

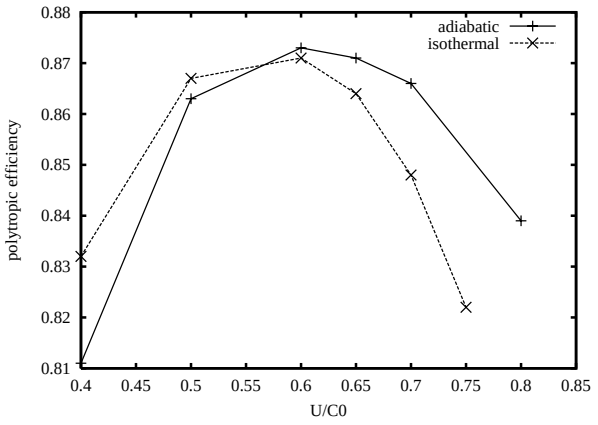

Fig.11: Polytropic efficiency of $\phi 4$ model (Wall temperature effect)

Work output and heat transfer at $U/C_0 = 0.6$ are listed in Table 2. Work output at the isothermal wall is always smaller than the adiabatic counterpart due to the energy loss at the wall. Comparing $\phi 4$ and $\phi 40$ at isothermal wall, the ratio of the heat transfer to the work output for $\phi 4$ model is about twice as much as that for $\phi 40$ model.

Influence on the efficiency In Figures 8 and 9, adiabatic efficiency evaluated at two wall conditions are compared for each model. The adiabatic efficiency is directly influenced by the decrease of temperature due to heat transfer at the wall. Therefore, as expected from the heat-transfer to work-output ratio in Table 2, the efficiency with isothermal wall is lower than that with adiabatic wall for all cases and the deterioration of effi-

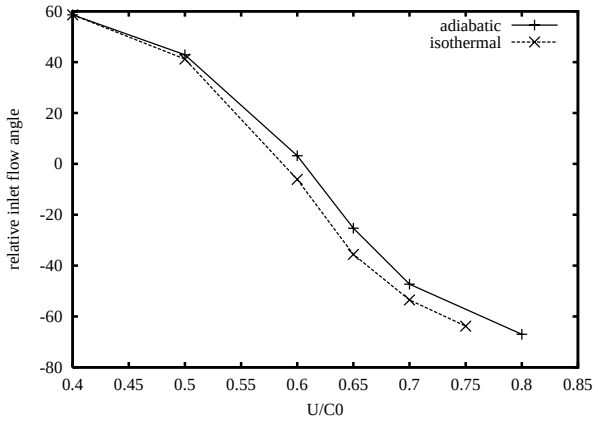

Fig.12: Rotor relative inlet flow angle of $\phi 4$ model

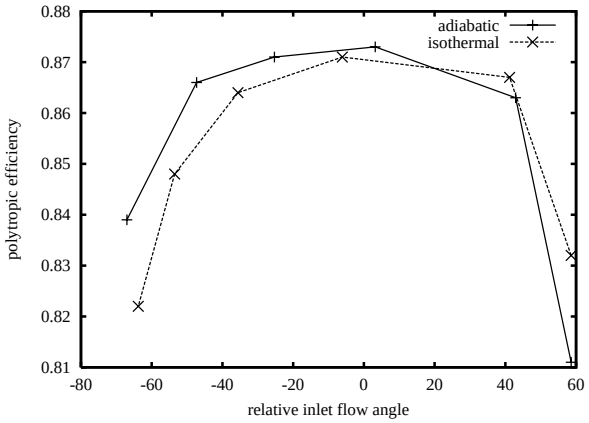

Fig.14: Polytropic efficiency of $\phi 4$ model (Wall temperature effect)

ciency is larger for $\phi 4$ model than $\phi 40$ model.

The effect of the heat transfer upon the flowfield may be discussed more clearly with the polytropic efficiency.

Figures 10 and 11 show polytropic efficiency of $\phi 40$ and $\phi 4$ models. Two curves in Figure 10 show similar characteristic, indicating that the efficiency with the isothermal wall is higher than that with the adiabatic wall. However, detailed observation of the flowfields yielded no evidence to reasonably explain this difference in efficiency. For this reason, it seems that the polytropic efficiency defined by Eq.(4) tends to give higher efficiency for cooled wall ($700K$ against the exhaust gas temperature $900K$).

Figure 11, on the other hand, looks very different from Figure 10. The curve with isothermal wall shifts to the left from that with adiabatic wall. The shift is explained

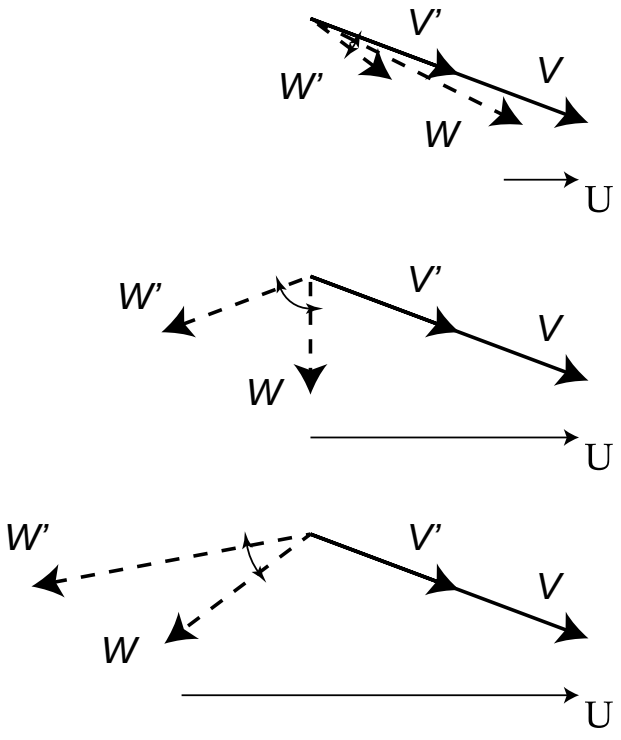

Fig.13: Mechanism of the inlet flow angle deviation

partly by the deviation of inlet flow angle.

Figure 12 shows the rotor relative inlet flow angle at each operation point. It indicates that the angle with isothermal wall deviates from the angle with adiabatic wall, especially, near $U/C_0 = 0.65$.

The deviation of relative inlet flow angle is caused by the decrease of flow velocity at the nozzle exit. Heat transfer at the walls lowers the total temperature and raises density, resulting in the lower flow velocity. It is shown from Figure 13 that deviation caused by the decrease of flow velocity depends on peripheral velocity U. There is a peak deviation near $U/C_0 = 0.65$ in this case.

This deviation of relative inlet flow angle should be considered at the design phase. Since the deviation is the largest near the design point in many cases, it is necessary to estimate heat loss in the nozzle and deviation of the rotor relative inlet flow angle.

Influence on the separation Figure 14 shows polytropic efficiency at $\phi 4$ model replotted against the rotor relative inlet flow angle. Two curves look more closer this time but there is still discrepancy at higher U/C_0 (negative relative inlet flow angle). The efficiency with the isothermal wall is lower than that with the adiabatic wall. This tendency cannot be explained by the deviation of relative inlet flow angle alone.

Flowfields at $U/C_0 = 0.7$ were investigated to figure out this phenomenon. Figure 15 shows Mach number contours at the rotor midspan, and Figure 16 shows streamlines around the rotor blade. These figures reveal that a separation region exists near the leading edge of the pressure side only with isothermal wall. It can be seen that the separation region near the trailing edge of the suction side with isothermal wall is larger than with adiabatic wall. The separation at the pressure side can be explained partly by the difference in the inlet flow angle, but the separation at suction side conflicts with the deviaiton of the inlet flow angle.

From these results above, it seems that separation is more likely to occur at the lower wall temperature. The operation range expected with isothermal wall may be,

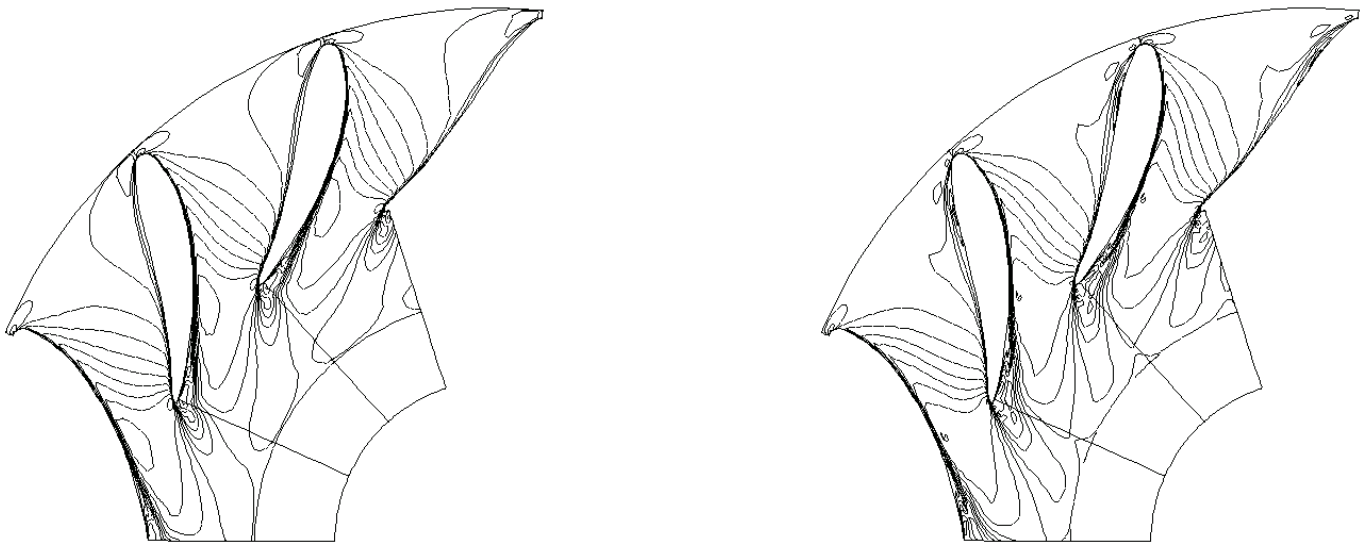

(a): adiabatic (b): isothermal

Fig.15: Mach number contours at the rotor midspan for $U/C_0 = 0.7$ (Wall temperature effect)

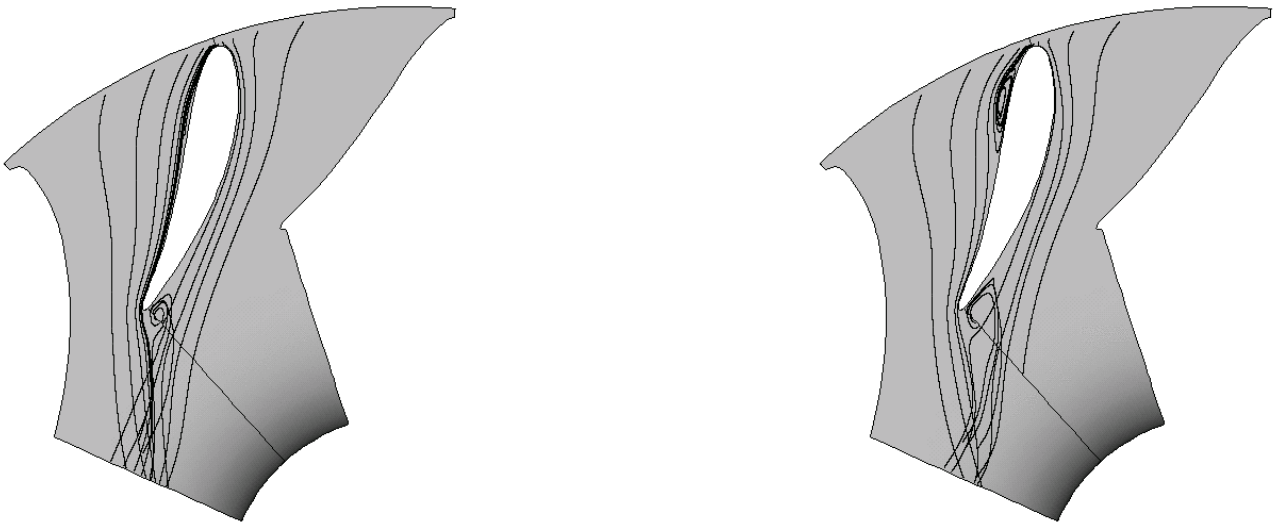

(a): adiabatic (b): isothermal

Fig.16: Streamlines around the rotor blade at the rotor midspan for $U/C_0 = 0.7$ (Wall temperature effect)

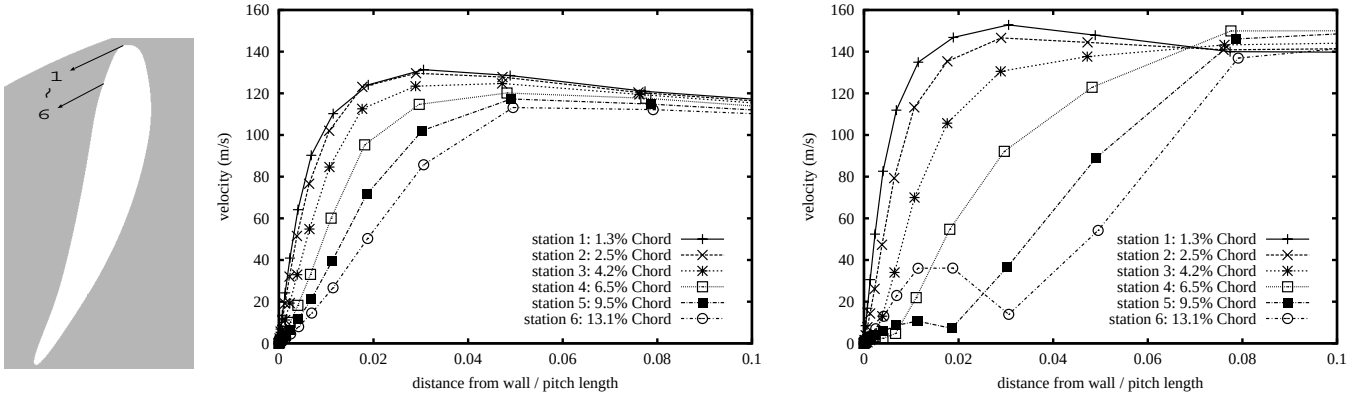

(a): adiabatic (b): isothermal

Fig.17: Velocity distribution inside the boundary layer near the leading edge of the rotor pressure side

for this reason, narrower than that with adiabatic wall.

Figure 17 compares the development of velocity distribution inside the boundary layer near the leading edge of the pressure side. With adiabatic wall, the boundary layer develops gradually from the leading edge. With isothermal wall, on the other hand, the velocity near the wall decrease rapidly as the boundary layer develops and then separation occurs. This result also indicates that heat transfer can have large impact upon the development of the boundary layer and therefore upon the flow separation.

CONCLUSIONS

Flowfield inside a micro turbine was numerically simulated. The influence of Reynolds number and heat transfer was discussed. As the Reynolds number decreases, the boundary layer becomes thicker and the efficiency drops, but no other remarkable change is found on the flowfield. It implies that miniaturization to this extent does not alter the characteristics of the flowfield dramatically. Heat transfer decreases the velocity at the nozzle outlet, so that the rotor relative inlet flow angle is varied. This deviation shifts the stage performance of the turbine. Development of boundary layer and separation is also influenced by the thermal boundary condition at the wall. The boundary layer on cooled wall is decelerated rapidly. It becomes more sensitive to the adverse pressure gradient and easily separates. These results indicate that performance estimation based on the conventional adiabatic wall condition is not adequate for shirt-button sized gas turbines and it is important to take into account the effect of heat transfer.

Acknowledgments

The present work was financially supported by NEDO International Joint Research Project (FY2001 No.5110159-0 and FY2002 No.0106013). The investigation is cooperated under a provisional committee of GTSJ for studying the minimization of gas turbine system.

References

Baldwin, B.S., and Lomax, H., "Thin Layer Approximation and Algebraic Model for Turbulent Flows", AIAA Paper 78-257,Jan. 1978.

A.H.Epstein, et al., "Micro-Heat Engines, Gas Turbines, and Rocket Engines", AIAA 97-1773

Eito Matsuo, Haruo YOSHIKI, Toshio NAGASHIMA and Chisachi KATO "Development of Ultra Micro Gas Turbines" Power MEMS 2002

Yves RIBAUD, "Overall Thermodynamic Model of an Ultra Micro Turbine", Proceedings of the Sixth International Symposium on Experimental and Computational Aerothermodynamics of Internal Flows, April 7-11, 2003, Shanghai, China, Volume 1, pp.86-90

Shima, E., and Jounouchi,T., "Role of CFD in Aeronautical Engineering (No.14)-AUSM Type Upwind Schemes", Proceedings of the 14th NAL Symposium on Aircraft Computational Aerodynamics, National Aerospace Lab., NAL SP-34, Tokyo, 1997, pp.7-12.

Obayashi, S., Matsushima, K., Fujii, K., and Kuwahara, K., "Improvements in Efficiency and Reliability for Navier-Stokes Computations Using the LU-ADI Factorization Algorithm", AIAA Paper 86-0338, Jan. 1986.